ISIJ International, Vol. 50 (2010), No. 12, pp. 1724–1734

Review

Methodological Progress for Computer Simulation of Solidification and Casting

Keiji NAKAJIMA,[1] Hongwei ZHANG,[2] Katsunari OIKAWA,[3] Munekazu OHNO[4] and Pär G. JÖNSSON[1]

1) Division of Applied Process Metallurgy, Department of Materials Science and Engineering, Royal Institute of Technology (KTH), Brinellvägen 23, SE-100 44, Stockholm, Sweden. 2) Key Laboratory of Electromagnetic Processing of Materials, Ministry of Education, Northeastern University, Wenhua Road 3-11, Shenyang, 110004, China.
3) Department of Materials Science, Tohoku University, 6-6-02 Aobayama, Aoba-ku, Sendai, 980-8579, Japan.
4) Division of Materials Science and Engineering, Graduate School of Engineering, Hokkaido University, North 13 West 8, Kita-ku, Sapporo, 060-8628, Japan.

(*Received on September 9, 2010; accepted on September 30, 2010*)

The dramatic progress made over the last 10 to 15 years in the field of "computer simulation of solidification and casting" is greatly due to the supports by academic as well as industrial research. The driving force behind this undertaking was the promise of predictive capabilities that will allow process and material developments. Here, the recent works on modeling were summarized, for the macrosegregation in the macro-scale simulation, and the Cellular Automaton, the solidification path combined with the microsegregation, the phase-field model in the meso-scale and micro-scale simulation.

KEY WORDS: solidification; casting; macrosegregation; cellular automaton; solidification path; microsegregation; phase-field model.

1. Introduction

The dramatic progress made over the last 10 to 15 years in the field of "computer simulation of solidification and casting" is obvious from the large numbers of publications after the review work by Stefanescu.[1] Especially, with the help of the *in-situ* synchrotron X-ray imaging technique for simulation validation, their accuracy in predicting various phenomena occurring during solidification and solidification microstructure at the end of solidification has been surely increased. However, the methodological progress is still in an unsatisfied state from the view point of practical use, although several approaches coupled with thermodynamic and kinetic databases have been done for multi-component alloys.

The purpose of "computer simulations of solidification and casting" is to generate a temporal and spatial description of the movement of the solid–liquid (S/L) interface, and consequently to predict the solidification microstructure related to product qualities and material properties. When simulating the solidification and casting phenomena according to that purpose, following four length scales must be considered, as shown in **Table 1**:

(1) The macroscopic-scale (macrostructure): it is in the order mm to cm and m. Subjects in the macroscopic-scale simulation include macrosegregation, shrinkage

Table 1. Length scales for simulations of solidification and casting.

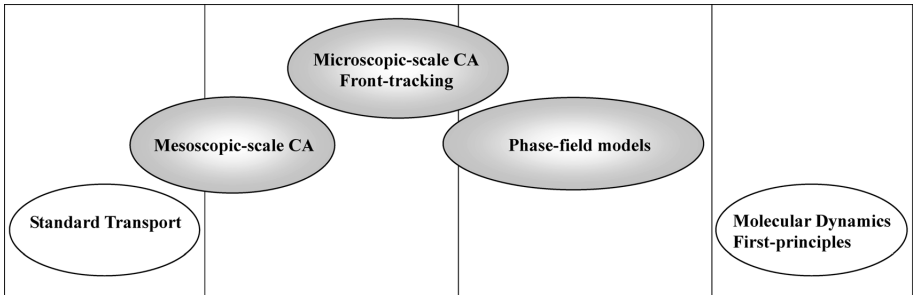

Macroscopic-scale	Mesoscopic-scale	Microscopic-scale	Nanoscopic-scale
(mm to *cm, m)*	*(μm* to *cm)*	*(nm* to *μm)*	*(~nm)*
Macrosegregation	As-cast grain structure (CET)	Growth morphology	Nucleation (Clustering)
Shrinkage cavity	Dendrite morphology (SDAS)	(Dendritic-type, Facet-type)	Interfacial energies
Cracks …	Microsegregation (Precipitation)	Microsegregation (Precipitation)	
	Transformation (Eutectic, Peritectic) …	Transformation (Eutectic, Peritectic)…	

cavity, cracks, *etc.* Product qualities, and their acceptance by the customers, can sometimes be dramatically influenced by these macrostructure features, especially macrosegregation.

(2) The mesoscopic-scale and microscopic-scale (microstructure): they are in the order μm to cm, and in the order of nm to μm, respectively. Subjects in the mesoscopic-scale and microscopic-scale simulation include the as-cast grain size and shape (columnar or equiaxed), the dendrite morphology (dendrite arm spacing), the microsegregation and consequent precipitation, *etc.* In most cases, material properties depend on the solidification structure at these scale levels.

(3) The nanoscopic-scale (atomic structure): it is in the order of nanometers (~nm).

An accurate description of the solidification nucleation, the S/L interface morphology, *etc.* requires atomistic calculations. The present knowledge and hardware development do not allow the application of the atomistic simulations in actual casting and solidification phenomena. However, recent methodologies in the mesoscopic-scale and microscopic-scale simulations require at least the nanoscopic-scale informations, such as solidification nucleation sites and interfacial energies,[2] during computation. The review work in nanoscopic-scale simulation was already done by Asta *et al.*[3]

Thus, this paper focuses on a modest attempt as reviewing a recent dynamic activity for the macrosegregation modeling in the macro-scale simulations, and the Cellular Automaton modeling, the solidification path combined with microsegregation modeling, the phase-field modeling in the meso-scale and micro-scale simulation, among various methods.

2. Macrosegregation Modeling (Macroscopic-scale)

Macrosegregation refers to defects in alloy castings with abnormal chemical compositional and/or microstructural changes in a scale lager than several millimeters. Macrosegregation is observed various casting processes. For a steel ingot casting process, A-segregation, V-segregation, bottom negative segregation, and hot top segregation are shown as typical macrosegregations in books for reference.[4] These macrosegregations are far more difficult to reduce subsequently by the thermo-mechanical treatments. Furthermore, they have significantly detrimental effects on various material properties. Therefore, the suppression of macrosegregation is one of the most important issues in the casting process research.

2.1. Channel Segregation Models

In this section, the "channel segregation" has been reviewed. The channel segregation shows a striking form and is observed in various castings such as, large ingots, vacuum-arc remelted ingots and directionally solidified ingots. The channel segregations are named by different terms in their morphology and processes. For example, the channel segregations in a vertical directionally solidification are commonly referred as "freckle segregations". On the other hand, streaks arranged in A-patterns in cast billets are called "A- or inverse V-segregation". It is widely recognized that the channel segregation is formed by a convective flow of a liquid in a mushy zone, resulting from the liquid density changes due to solutal and thermal gradient. Therefore, the channel segregation has been the subject of intense research in theoretical analysis and numerical simulations. Pioneering works of the channel segregation were Flemings *et al*. in 1960s.[5,6] They considered the flow of liquid in the mushy zone caused by shrinkage, and proposed the following modified Scheil equation:

$$\frac{df_S}{dC_L} = \frac{1-f_S}{C_L}\frac{1-\beta}{1-k}\left[1+\frac{v\cdot\nabla T}{\varepsilon}\right], \quad \text{.....(1)}$$

where f_S is the solid volume fraction, k is the partition coefficient, C_L is the solute concentration in the liquid, β is the solidification shrinkage, v is the velocity vector of the liquid, ∇T is the temperature gradient, and ε is the cooling rate. This simple equation could explain the formation mechanism of several kinds of macrosegregation. If the term in the square bracket in Eq. (1) becomes negative, the solid fraction decreases, which is the cause of the open channels in the mush that lead to the channel segregation. After this study, several analytical models have been proposed.[7–11] For instance, Mehrabain *et al.*[8] considered the natural convection as well as the shrinkage-driven flow. However, these analyses were conducted under the limited conditions, such as a steady-state flow. In addition, considerable progress in understanding the macrosegregation has been achieved by numerical simulation models that couple mass, momentum, energy, and species in all regions (solid, mushy and bulk liquid), and also succeeded in predicting freckles qualitatively.[12] These approaches also considered the microscopic scale models, such as microsegregation and permeability models. Well-documented reviews of the macrosegregation modeling are available in the literature.[13,14] These multi-scale models linked the channel segregation and microscopic parameters. Microscopic models and numerical schemes to reduce computational burden have also still been developed, especially the model of the back diffusion, permeability term. Also, there has recently been intense interest in development of models for the industrial multi-component alloy coupled with thermodynamic phase equilibrium[15] and a three-dimensional (3D) system to compare directly with experimental data.[16] The example of 3D simulation result directly compared with the experimental result is shown in **Fig. 1**.[17] The predicted shape and position of the channel segregation shows good agreement with the experimental result.

2.2. Channel Segregation Formation Criteria

Several channel segregation formation criteria to selecting solidification conditions for minimizing them have been proposed based on the experimental and simulation results. In the viewpoints of thermal conditions, thermal gradients (G) and solidification rates (R) have been used as the channel segregation formation criteria.[18—20] Coply *et al.*[18] suggested a critical cooling rate ε (ε equal to $G\cdot R$) for the channel segregation formation based on the vertical directional solidification results of the NH_4Cl–H_2O system. Suzuki and Miyamoto[19] carried out the lateral directional solidification of various high carbon steels. Based on a phe-

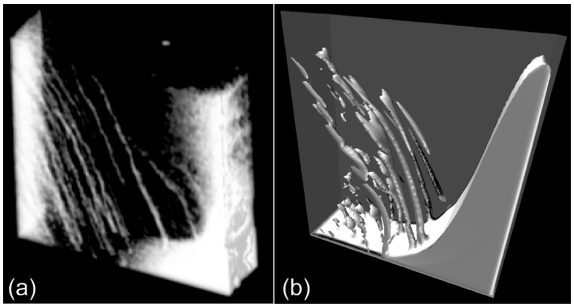

Fig. 1. Comparison of three dimensional simulation and experimental result of lateral directional solidification of Sn–20mass%Bi alloy. (a) Iso-surface at Bi segregation ratio 1.0 of numerical result and (b) stereoscopicstructure of channel segregation by X-ray CT-image.[17]

nomenological analysis of their experimental data, they proposed a critical solidification conditions as $G \cdot R^{2.1} < 8.75$ or $\varepsilon \cdot R^{1.1} < 8.75$. Pollock and Murphy[20] preformed the vertical directional solidification of Ni-base superalloys and found the critical primary dendrite arm spacing for the channel segregation formation. According to traditional theories, the primary dendrite arm spacing varies with $G^{-1/2} \cdot R^{-1/4} < 0.95$, they suggested this thermal parameter as an improved channel segregation criterion. These criteria show the similar type of equation, although the exponential factors are different. The reason for these differences has not been clarified yet. It is considered that the experimental conditions such as ingot size and gravity direction would influence the formation of the channel segregation.

Several investigators have attempted to characterize their experimental results in terms of a musy-zone Rayleigh number, which suggests the instability of the buoyancy-driven flow in a mushy-zone.[21–25] Beckerman *et al.*[26] suggested that the mushy-zone Rayleigh number definitions proposed by Worster[25] is physically most meaningful, although several different definitions have been proposed. His definition is given by

$$Ra_{\mathrm{crit}} = \frac{(\Delta\rho/\rho_0)gKh}{\alpha\nu} < \text{constant} \quad \text{.....(2)}$$

where h is the height of the mushy zone, $\Delta\rho/\rho_0$ is the density gradient in the liquid, K is the average permeability, g is gravitational acceleration, α is the thermal diffusivity, ν is the kinematic viscosity of the liquid in the mushy zone. The main advantage of this criterion is that the influence of alloy composition can be taken into account by $\Delta\rho/\rho_0$. Since K and h depend on the cooling rate and thermal gradient, respectively, Beckermann *et al.*[26] suggested that the relation between this mushy zone Rayleigh number and the thermal criteria is given as

$$Ra_{\mathrm{crit}} \sim R^{-2/3} \cdot G^{-5/3} < \text{constant, or } G^{-1/2} \cdot R^{-1/5} < \text{constant} \quad \text{.....(3)}$$

This inequality suggests that the Rayleigh number criteria include the thermal criteria indirectly. Furthermore, Beckermann *et al.*[26] showed the linear relationship between the Rayleigh number and thermal criteria based on experimental results of Pollock and Murphy[20] as shown in **Fig. 2**. Recently, Kajikawa *et al.*[27] showed that the thermal criteria values evaluated by Suzuki and Miyamoto's method depend

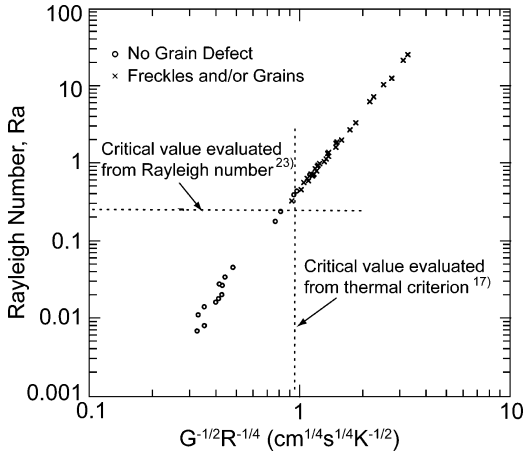

Fig. 2. Calculated mushy zone Rayleigh number for the vertical directional solidification experiments of Pollock and Murphy[20] as a function of solidification parameter $G^{-1/2} \cdot R^{-1/4}$.[26]

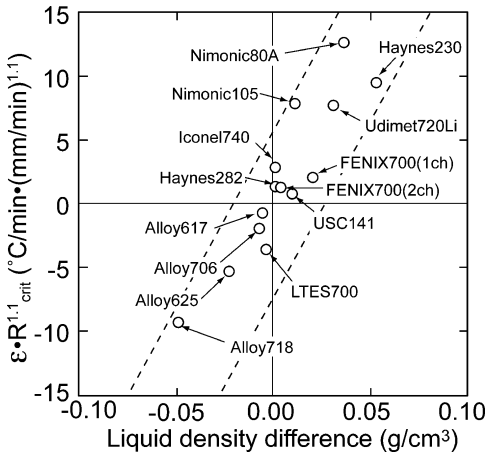

Fig. 3. Relation between liquid density difference and the critical value of thermal criteria of Ni-base superalloys obtained by Suzuki and Miyamoto's method.[27]

on the alloy composition. Futhermore, that they show nearly a linear relation between the critical values and the liquid density difference, $\Delta\rho$ as shown in **Fig. 3**. Since $\Delta\rho$ is the variable of the Rayleigh number, this result also suggests that there is strong relation between the Rayleigh number criteria and the thermal criteria.

Recently, Sawada *et al.*[28] numerically analyzed the vertical directional solidification of Pb–10mass%Sn alloys to examine the growth mechanism of the channel segregation. The channel segregation was always open to the bulk liquid from its generation, and did not confirm obvious remelting phenomenon in the simulation grid scale. Detailed investigation of the effects of convection on the growth of channel segregation showed that a solidification-accelerated region and solidification-retarded region were formed by the convection near the solidification front as shown in **Fig. 4**. At the solidification-accelerated region, solidification was accelerated by the inflow of lower Sn concentration liquid from the bulk liquid. Since the Sn concentration of liquid in the mushy zone increase with the progress of the solidification, the solidification was retarded near the channel by inflow of the liquid from the solidification-accelerated region. As the results, the growth of channel segregation is empha-

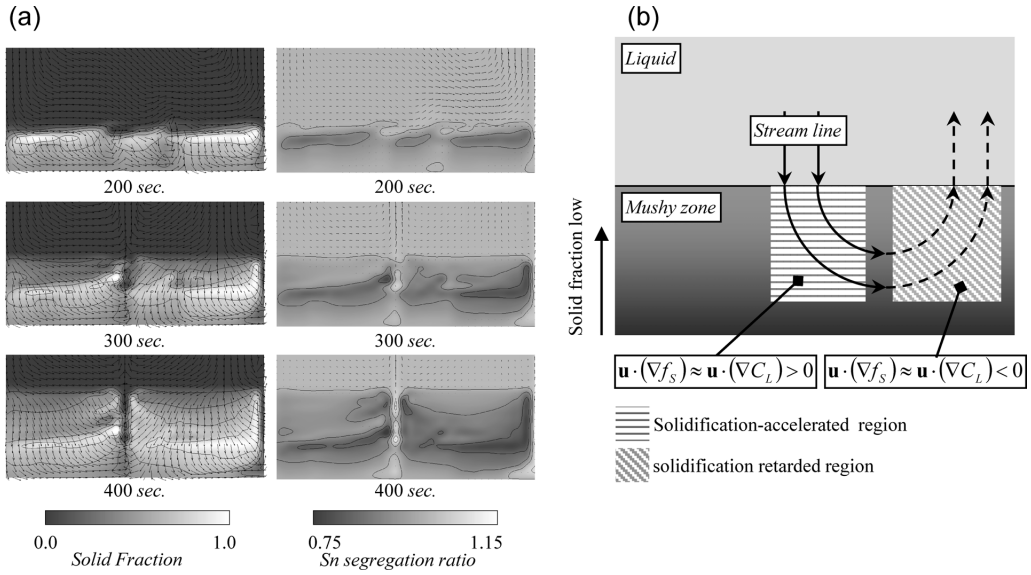

Fig. 4. (a) Simulation results of Pb–10mass%Sn alloy vertical solidification. Distribution and contours of solid fraction (left) and Sn segregation ratio (right) for channel growth. (b) Schematic view of the coupled solidification-accelerated region and solidification retarded region which form at solidification front and flow field.[28)]

sized by the coupling of solidification-accelerated region and solidification-retarded region.

2.3. Summary

The numerical simulations of macrosegregation have elucidated the formation of the channel segregation. However, it is still difficult to apply these numerical simulations to the practical size ingots and slabs for ingot casting and the continuous casting processes due to inadequate computing power. Development of numerical techniques will be necessary for industrial applications. Furthermore, the progress of numerical models, especially such as flagmentation and movement of solid phase by fluid flow, will be required to predict various kinds of macrosegregation phenomena.

3. Cellular Automaton Modeling (Mesoscopic-scale and Microscopic-scale)

Cellular Automaton (CA) is an efficient tool to predict the solidification grain structures in ingot, billet, slab, *etc.* with combinations of the probabilistic and the deterministic approaches. Firstly, Gandin *et al.*[29–36)] developed mesoscopic-scale CA (in the order μm to cm), which can model the columar-to-equiaxed transition (CET) as well as the grain structure by solving each individual grain growth. This is done through a coupling with macroscopic heat and solute transport equations (deterministic approach). Afterwards, Dilthey and Pavlik,[37)] Nastac,[38)] Beltran-Sanchez and Stefanescu,[39,40)] and Zhu *et al.*[41–48)] developed microscopic-scale CA (in the order of nm to μm), which can simulate the detailed dendritic structure. With the development of these two scale CA, many complicated phenomena occurring in the solidification process have been described and drawn; such as the competitive growth of multi-grains with different crystallographic orientations (selection of columnar grains), the deflection behavior of columnar grains solidified in a flowing melt, the secondary dendrite arm spacing (SDAS), the microsegregation of binary, ternary and multicomponent alloys, the eutectic microstructure and the extension into 3D case.

3.1. Grain Nucleation Models

It is assumed that heterogeneous nucleation of solidification grains takes place on particles present in the melt. Such heterogeneous nucleation events are described by the following two major models,[1,49)] although they are still empirical in essence owing to use of adjustable parameters. One is the instantaneous nucleation model, which is effective for a saving of computational time in the system in the presence of melt convection or for a 3D case. It assumes an abrupt burst of nucleation as soon as a critical undercooling is reached.[32,34–36)] Another one is the continuous nucleation model which assumes a continuous temperature dependence of the nucleation density. Since several families of nucleation sites, all characterized by different critical undercoolings, usually coexist in the melt, this seems to be more realistic. In Oldfield's continuous model,[50)] a power-law function was used to evaluate the nucleation rate. For less adjustable parameters, Ohsasa *et al.*[51,52)] adopted this continuous model in several of their CA simulations. In Thevoz *et al.*'s continuous model,[53)] a statistical function, that is, a Gaussian distribution of nucleation density with undercooling for the nucleation site distribution was used,

$$\frac{dn}{d(\Delta T')}=\frac{n}{\sqrt{2\pi}\cdot\Delta T_\sigma}\exp\left[-\frac{1}{2}\left(\frac{\Delta T'-\Delta T}{\Delta T_\sigma}\right)^2\right]. \quad ...(4)$$

Two different types of adjustable parameters are used for the heterogeneous nucleation at the mold wall (n_S, ΔT_S, $\Delta T_{S,\sigma}$) and in the bulk of liquid (n_V, ΔT_V, $\Delta T_{V,\sigma}$), where n is the maximum nucleation density, ΔT and ΔT_σ are the maximum undercooling and the standard deviation of the nucleation distribution, respectively. It is noticed that the limit condition $\Delta T_\sigma \rightarrow 0$ K in Thevoz *et al.*'s continuous model corresponds to the instantaneous nucleation model. Gandin *et al.*[29,30)] and Nakajima *et al.*[54—56)] adopted this continuous model in several of their CA simulations. Futhermore, judged the activation level (nucleation probability) of each

CA cell by using Eq. (4). That is to say, during one micro time step δt, if the nucleation probability of a CA cell $P_V = dn \cdot V_{CA}$ is greater than a random number, the CA cell is nucleated (V_{CA} is the volume of a CA cell); dn is the increase of nucleation density corresponding to an undercooling increase $d(\Delta T)$. Once nucleated, the CA cell's state is changed from liquid to solid, and it is given a random crystallographic orientation.

3.2. Grain Growth Models

The grain growth models are classified into two major models: those based on the evolution of the grain envelope (in mesoscopic-scale CA), and those based on the evolution of the S/L interface (in microscopic-scale CA).

3.2.1. Mesoscopic-scale CA (Grain Envelope Evolution)

The grain in a mesoscopic-scale CA is defined as the "envelope" outlined by the dendrite arm tips. Thus, mesoscopic-scale CA simulates the evolution of the external envelop for grains during solidification, but does not simulates the evolution of the S/L interface itself.

The steady-state growth kinetics of the dendrite tip is analytically deduced as a function of the local undercooling, *i.e.* the sum of solutal, curvature and thermal undercoolings.[57,58] When the local undercooling is regarded only as the contribution of solutal undercooling, the growth kinetics is described by the KGT[59] or the LKT model.[60] Recently, the GGAN model[33,34] was developed by considering the contributions of solutal and curvature undercooling in the presence of fluid flow. It can calculate just a dendrite tip growth velocity as a function of both the intensity and the orientation of the fluid flow with respect to the dendrite growth direction.[61] For computational efficiency, most researchers use a simplified form (using either a polynominal law or a power law) of the above growth kinetics by a direct interpolation of the velocity versus the undercooling relationship.

According to the above growth kinetics, the nucleated grain starts to grow up in a envelope shape. Its neighbor cell (Moore neighbourhood rather than Von Neumann neighbourhood) tends to be entrapped, once the cell center is located inside this growing envelope. Gandin *et al.*[29–31] has developed three kinds of grain growth algorithms in a mesoscopic-scale CA. One is the "square" growth algorithm[29] in which both nucleation grains and entrapped grains grow in a square envelope in a two-dimensional (2D) case. It can only be applied to uniform temperature fields. Since the grain orientation is strongly biased by the artificial anisotropy of CA mesh system, a "dendrite tip correction" should be done to keep the original crystallographic orientation of grains. The subsequent one is the "rectangle" growth algorithm[30] in which the nucleation grains grow in a square envelope, while the entrapped grains grow in a rectangular envelope in a 2D case. It can maintain the original grain orientation without "correction" and can be applied to non-uniform temperature fields. However, it is difficult to extend the simulation to a 3D case. Therefore, the result is a "decentred square" growth algorithm[31] in which both nucleation grains and the entrapped grains grow in a square envelope in two dimensions. In the algorithm, the square envelope is always truncated to a proper size to avoid overgrowth. Thus, the virtual growth center for the cell usually biases its center in the CA network. The "decentred square" growth algorithm can maintain the original grain orientation. Futhermore, it can describe more exactly the development of the solidification microstructure in a non-uniform temperature field and can easily be extended to the "decentred octahedron" growth algorithm[31,32] for a 3D case. Even in the presence of fluid flow, where each dendrite tip growth velocity is different due to both the effects of the intensity and the orientation of the fluid flow with respect to the dendrite growth direction, it results in the "irregular decentred-quadrilateral" growth algorithm for a 2D case.[34–36,61] Recently, using the third algorithm, Gandin *et al.* proposed the coupled Cellular Automaton-Finite Element (CA-FE) model, for the prediction of the interaction between the formation of the grain structure and the macrosegregation. This was additionally coupled with the calculation of a solid and liquid flow induced macrosegregation. The movement of the solid phase (for example, the transport and sedimentation of equiaxed grains) generates a movement of the liquid phase and the transport of all quantities that needs to be accounted for at the scales of the CA cell and the FE mesh. The model is applied to simulate the solidification of a Pb–48mass%Sn alloy[34,36] and a Ga–5mass%In binary alloy.[35] The predicted shape and position of the channel segregation by the simulation shows a good agreement with the experimental results, as shown in **Fig. 5**.

3.2.2. Microscopic-scale CA (Dendritic Growth Evolution)

Microscopic-scale CA simulates the evolution of the S/L interfaces. That is the dendritic growth morphology itself. For the microscopic-scale CA for dendritic growth, two major types can be distinguished: those based on the steady-state growth kinetics of the dendrite tip and those based on numerical solutions including the boundary conditions at the S/L interface.

The microscopic-scale CA based on the steady-state growth kinetics of the dendrite tip solve the heat and solute transport equations on a CA mesh. The corresponding values of the composition and temperature at each mesh point are then used to obtain the local undercooling. This, in turn, defines a unique velocity of the S/L interface based on the steady-state growth kinetics of the dendrite tip (the KGT[59] or the LKT model[60]). A basic assumption in these models is that the motion of any point of the dendritic S/L interface at any time follows the same functional dependency as that of the tip at steady state. This type of microscopic-scale CA has been applied by Zhu and Hong[41–44] to simulate 2D and

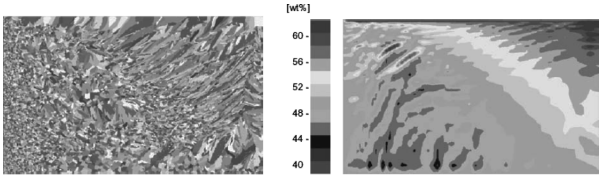

(a) (b)

Fig. 5. Prediction from meso CA-FE model for a Pb–48mass%Sn alloy in a parallelepipedic cavity 100 mm×60 mm. (a) Final grain structure. (b) Segregation map of tin with its composition scale.[36]

3D single and multi-dendritic growth,[41,42] dendritic growth in the presence of melt convection,[43] and microstructure formation in regular and irregular eutectics alloys.[44] Thus, this technique may be used to simulate a wide variety of experimentally observed microstructures in alloy solidification. However, in this type of microscopic-scale CA, the velocity of the S/L interface is calculated from the steady-state growth kinetics of the dendrite tip. This approximation leads to mostly qualitative graphical outputs.

The microscopic-scale CA based on the heat and solute transport equations includes the boundary conditions at the S/L interface that define the problem of dendritic growth, *i.e.* local equilibrium and conservation of heat and solute. This type of microscopic-scale CA affords the distinct advantage of avoiding the introduction of the steady-state growth kinetics of the dendrite tip to calculate the interface velocity. However, in order to produce the dendritic features of side branching, local noise (small random perturbations) must be introduced into the calculation of the solid fraction evolution at the S/L interface or in the capturing step of new interface cells. The earlier trials of Dilthey and Pavlik[37] and Nastac[38] suffers from the strong artificial anisotropy of the CA mesh. All the simulated dendrites grow aligned with the mesh axis. Afterwards, Belteran-Sanchez and Stefanescu[39,40] solved this problems of mesh-induced anisotropy in crystallographic orientation, using a virtual tracking scheme of the sharp S/L interface for simulation of the dendrite growth in the low Peclet-number regime.

In order to conquer the above weakness in previous microscopic-scale CA, Zhu and Stefanescu[45] proposed newly a 2D front-tracking (FT) model for the simulation of dendrite growth in the low Peclet-number regime. In this new method, the kinetics of the S/L interface evolution is determined using a local interface composition equilibrium approach. This allows an accurate simulation of dendrite growth from the initial unstable stage to the steady-state stage without the need of the steady-state growth kinetics of the dendrite tip. In addition, this method adopts a virtual interface-tracking scheme previously proposed by Beltran-Sanchez and Stefanescu[39,40] to explicitly capture the new interface cells. The exact S/L front is implicitly scaled by the solid fraction within each interface cell. This hybrid scheme facilitate a straight forward handling of complex topology changes, while the concept of a sharp transition between the liquid and solid is maintained. Later, this new method was extended by Zhu *et al.*[46,47] to include the presence of melt convection with the help of lattice Boltzmann method (LBM), and to a 3D case, as shown in **Fig. 6**.

3.3. Summary

The mesoscopic-scale CA treats the evolution of the grain envelope, for directly simulations of the solidification grain structure in ingots, *etc.* Recently, it started to reach the prediction of the interaction between the formation of the grain structure and the macrosegregation case.[34–36] Meanwhile, the microscopic-scale CA treats the evolution of the S/L interface for closely simulating the dendritic structure, the microsegregation, the eutectic microstructure, *etc.* It has been bridging the gap between the phase field model and the above mesoscopic-scale CA. Recent significant challenge might be its application to multi-component alloy systems.[48]

4. Solidification Path Combined with Microsegregation Modeling

During the solidification process, the appearance sequence of the phases and the temperature change of both the amounts and the compositions of each phase are generally called the "solidification path". The prediction of the solidification path has to be combined with a certain microsegregation model. There are many microsegregation models proposed for the prediction of solidification path, as shown in **Table 2**.

4.1. Fundamental Microsegregation Models in Software Packages

There are several commercial software packages, such as Thermo-Calc, Pandat, MatCalc, ChemAPP, TerFKT, PmlFKT, *etc.*, which can predict the solidification path according to the Lever Rule (LR, infinite diffusion in solid), Gulliver–Scheil model[62–65] (GS, no diffusion in solid), and the Partial Equilibrium model proposed by Kozeschnik[66] and Chen and Sundman[67] (PE, infinite diffusion of interstitial solutes and no diffusion of substitutional solutes in solid), respectively. These three models assume a uniform solute distribution in the liquid, which is reasonable for a large diffusivity and in the presence of flow. For the solid, the LR assumes that the solute diffusion is also so rapid that a uniform composition is maintained, which is reasonable only for interstitial solutes like C, O and N. On the other hand, for substitutional solutes in the solid, diffusion is much slower and can often be neglected. This is the other

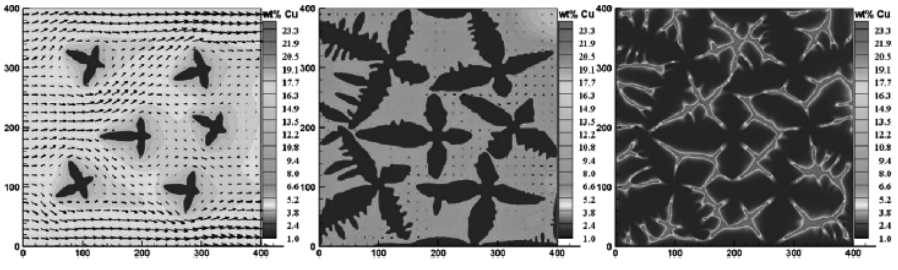

(a) (b) (c)

Fig. 6. Evolution of multiequiaxed dendrites for an Al–4.5mass%Cu alloy solidified in a square domain 88 μm×88 μm with a cooling rate of 10 K/s and a forced flow with an inlet flow velocity 0.001 m/s. (a) Solid fraction f_s=0.06, (b) f_s=0.45, (c) f_s=0.93.[46]

Table 2. Microsegregation models for prediction of solidification path.

Model	Diffusion in liquid	Diffusion in solid	Dendrite arm spacing	Cooling rate	Binary/Multi-component	Solidification Structure	Convection	Method
Lever rule	Infinite	Infinite	No	No	Multi-component	Liquid +solids	No	Thermodynamic Equilibrium Calculation by Commercial Software (TECCS) (Thermo-Calc, Pandat, MatCalc, ChemAPP, TerFKT, PmlFKT, etc)
Gulliver/Scheil [62-65]	Infinite	No	No	No	Multi-component	Liquid +solids	No	TECCS (Thermo-Calc, Pandat, MatCalc, ChemAPP, TerFKT, PmlFKT, etc)
Kozeschnik /Chen (Partial Equilibrium) [66,67]	Infinite	Interstituals: Infinite, Substatutionals: No	No	No	Multi-component	Liquid +solids	No	TECCS (MatCalc, Thermo-Calc)
DICTRA [68]	Limited	Limited	Yes	Yes	Multi-component	Liquid +2 solids	No	TECCS (Thermo-Calc)
Kobayashi [70-73]	Infinite	Limited	Secondary dendrite arm spacing	Yes	Multi-component	Liquid +dendritic +peritectic	No	Analytical model
Beckermann [74-76]	Limited	Limited	Secondary dendrite arm spacing	Yes	Binary	Liquid +dendritic	Yes	Numerical model
Gandin [77-79]	Limited	Limited	Secondary dendrite arm spacing	Yes	Binary Ternary	Liquid +dendritic +eutectic, Liquid +dendritic +peritectic +eutectic Liquid +dendritic	Can be combined	Numerical model + TECCS (Thermo-Calc)
Krane [80]	Infinite	Infinite	No	Yes	Ternary	Liquid +dendritic +peritectic +eutectic	Yes	Numerical model + equilibrium phase diagram
Pustal [81]	Limited	Limited	Secondary dendrite arm spacing	Yes	Ternary	Liquid +dendritic +eutectic	No	Numerical model + TECCS (Thermo-Calc)
Combeau [82,83]	Limited	Limited	No	Yes	Multi-component	Liquid +dendritic +peritectic	Can be combined	Numerical model + TECCS (Thermo-Calc)
Natsume [84]	Limited	Limited	Secondary dendrite arm spacing	Yes	Binary, multi-component	Liquid +dendritic +peritectic	No	Numerical model + TECCS (ChemAPP)

(Note) Previous analytical microsegregation models that were presented before the exact analytical solution of the Brody-Felemings equation by Kobayashi[70-73] can be found in the review work by Stefanescu[1].

basic assumption of the GS model. The GS model is sound for Al-based and Ni-based alloys. Meanwhile, for steels, a more realistic approximation is a partial equilibrium, *i.e.* complete interstitial but negligible substututional solute back difuusion in the solid. This is realized in the PE model[66,67] through evening up the chemical potential of the interstitials throughout the solid. In above software packages, the prediction of the solidification path for various alloys is available through coupling with these three models and thermodynamic and kinetic database. However, the assumption of infinite diffusion in the liquid might lead to a false result.

Another software package DICTRA,[68] including a kinetic database MOB2[69] can also predict the solidification path. Here, the solidification behavior under local equilibrium conditions is assumed to be controlled by the solute diffusion in both the liquid and the solid. In addition, the exact analytical solution of the Brody–Flemings equation by Kobayashi[70–73] should be introduced here, since it is not included in any commercial software packages today.

4.2. Other Microsegregation Models

A comprehensive theoretical treatment of dendritic growth requires an accurate tracking of the solutal field during the solidification. In this stand point, many other micro segregation models were proposed.[74–84] A summary of major assumptions used in these micosegregation models is given in **Table 2**.

Beckermann *et al.*[74–76] proposed a microsegregation model for the equiaxed solidification of binary alloys, which considers the formation of a primary dendritic structure into an undercooled liquid. Three phases within a representative elementary volume: solid, interdendritic liquid and extradendritic liquid are defined. Thereafter, the limited diffusion in each phase is taken into account. This model includes the effects of the secondary dendrite arm spacing and the cooling rate, which are the two major factors influencing the solidification path. In addition, Gandin *et al.*[77–79] extended this microsegregation model to consider the formation of a concurrent dendritic and eutectic structure[77]

and further a concurrent dendritic, peritectic and eutectic structure[78] up to the completion of a binary alloy solidification process. Furthermore, the model has been extended to include the prediction of a primary dendritic solidification of a ternary alloy system,[79] by coupling of thermodynamic and kinetic databases. This ternary-alloy model is easily extended to multi-component alloys.

4.3. Summary

The use and limitation of various microsegregation models proposed for the prediction of solidification path are briefly described. From the view point of an accurate prediction of the appearance sequence of the phases and the temperature change of both the amounts and the compositions of each phase, Gandin *et al.*'s model[77–79] should at present be recommended. Meanwhile, the combination of a microsegregation model with the macroscopic heat and solute transport equations is an efficient way for prediction of both the solidification path and the solidification grain structure. From another point of view, for simulations of actual castings,[54] Kobayashi's model[70–73] and Natsume's model,[84] based on a one-dimensional case, should presently be recommended.

5. Phase-field Modeling (Microscopic-scale)

The phase field model has emerged as a powerful computational tool to simulate microstructural evolution processes during phase transformation phenomena.[85–89] In the field of solidification and casting, this model has attracted much attention, since quite impressive outcomes of the dendrite structure were demonstrated by Kobayashi,[90,91] Wheeler *et al.*[92] and Warren and Boettinger.[93] The development of the alloy solidification model by Kim *et al.*[94] and the multi-phase-field model by Steinbach *et al.*[95] represent important works in phase-field modeling. The solidification is essentially the non-equilibrium process involving the temporary evolutions of non-uniform distributions of the temperature field, the fluid field and the concentration field. The description of the solidification microstructure requires coupling of these fields to be properly described. Here, the phase-field model can explicitly deal with the couplings of these fields. Therefore, the phase-field model has been applied to simulation of a variety of microstructural evolution processes during the solidifications in many systems. More specifically, for example the single phase solidification for pure substance and binary alloy systems,[96–98] and the solidification process for multicomponent and multiphase alloy systems.[99–107] The important works on the phase-field modeling and their applications can be found in several review articles.[85,87–89] Here, we briefly review the recent development of the quantitative phase-field model.

5.1. Quantitative Phase-field Model for Solidification

The motion of the solid-liquid interface has been tackled in the theoretical framework called the free boundary problem (FBP). When the isothermal solidification process in an alloy system is considered, the FBP corresponds to the problem of finding the solution of the diffusion equations in each bulk phase, the mass conservation law at the interface and the Gibbs–Thomson relation. The diffusion equation is given as,

$$\frac{\partial c}{\partial t} = D_i \nabla^2 c \ , \quad \text{.....(5)}$$

where c is the concentration of solute atom and D_i is the diffusion coefficient of the solute atom in the i-th phase. Also, the mass conservation law at the interface can be written as,

$$c_l^*(1-k)V = D_s \frac{\partial c_s}{\partial n}\bigg|^* - D_l \frac{\partial c_l}{\partial n}\bigg|^* \ , \quad \text{.....(6)}$$

where V is the migration velocity of the interface, k is the partition coefficient, c_s and c_l are the concentration in the solid and liquid phases, respectively. Furthermore, c_l^* represents the concentration in the liquid phase at the solid–liquid interface and n is the spatial coordinate normal to the interface. The spatial derivative on the right-hand side of Eq. (6) was evaluated at the interface. The Gibbs–Thomson relation is expressed as,

$$T = T_{\mathrm{m}} - |m| c_l^* - \Gamma \cdot \kappa - V/\mu \ , \quad \text{.....(7)}$$

where T_{m} is the melting temperature at $c=0$, m is the liquidus slope, Γ is the Gibbs–Thomson coefficient, κ is the curvature of the interface and μ is the linear kinetic coefficient. For an isothermal solidification process at T_0, this relation may be rewritten as,

$$c_l^* / c_l^e = 1 - (1-k)d_0\kappa - (1-k)\beta V \ , \quad \text{.....(8)}$$

where c_l^e the equilibrium concentration of the liquid at T_0, d_0 is the chemical capillary length defined by $d_0 = \Gamma/\Delta T_0$ with $\Delta T_0 = |m|(1-k)c_l^e$ and β is given as $\beta = (\mu \Delta T_0)^{-1}$. Within the FBP, the solid–liquid interface is regarded as a boundary without the thickness and the position of the interface is tracked. This approach becomes quite cumbersome when the morphology of the phase is complex. On the other hand, the phase-field approach is based on the diffuse-interface concept. Here, the interface is expressed as the inhomogeneous localization of the state variable called the phase-field. Hence, the phase-field model allows us to avoid explicit tracking of the moving phase boundaries in complex patterns. This is in marked contrast to the computational methods based on sharp-interface descriptions.

Within the phase-field model, the morphology of the solidification microstructure is characterized by the phase-field, as mentioned above. This field is denoted by p, and is equal to 1 in the bulk solid phase and equal to 0 in the liquid phase. Then, the interface region is characterized by the continuous variation of p from 0 to 1. The time evolutions of p and c are described based on the total free energy in the system. More specifically, by the Ginzburg–Landau-type free energy functional, which is expresses as,

$$F = \int_V \left[\frac{\varepsilon^2}{2} (\nabla p)^2 + f^0_{\mathrm{bulk}}(p,c) \right] dV \ , \quad \text{.....(9)}$$

where ε is the gradient energy coefficient, f^0_{bulk} is given by,

$$f^0_{\mathrm{bulk}}(p,c) = \omega \cdot f(p) + g(p) f_s(c_s) + (1-g(p)) f_l(c_l) \ \ldots(10)$$

Here, ω represent the potential height between the bulk phases, f_s and f_l are the local free energy density of the solid

and liquid phases, respectively. Also, $f(p)$ and $g(p)$ are the interpolating functions introduced to describe the thermodynamic state between the liquid and solid phases. The time evolution of the concentration is described by the following diffusion equation,

$$\frac{\partial c}{\partial t} = -\nabla \mathbf{J}_c = -\nabla\left(-M_c \nabla \frac{\delta F}{\delta c}\right), \quad \text{.....(11)}$$

where M_c is the mobility related to the diffusion coefficient. The time evolution of the phase-field is described by the time-dependent Ginzburg–Landau equation for a non-conserved quantity,

$$\frac{\partial p}{\partial t} = -M_p \frac{\delta F}{\delta p}, \quad \text{.....(12)}$$

where M_p is the phase-field mobility. In the phase-field model for the solidification, several phenomenological descriptions and assumptions are introduced. Therefore, its output carries a quantitative meaning only when the model can be precisely mapped onto the free-boundary problem of interest.

In the so-called sharp-interface limit, where the interface thickness W is taken to approach zero,[108–112] the phase-field model reproduces to a free-boundary problem when one holds a relation between measurable quantities and the parameters of the phase-field model. However, such a sharp-interface limit model makes it virtually impossible to describe the phenomena on an experimentally relevant spatial and temporal scales. This is due to the variable W. Thus, the computational grid spacing Δx and the time constant for the simulation need to be quite small compared to the typical scales of the microstructural pattern to obtain the results independent on the variable W. Karma and Rappel developed a seminal approach to resolve this problem for the solidification of pure materials with equal thermal diffusivities in the solid and liquid phases (a symmetric model).[113,114] They developed the model based on the thin-interface limit in which the free-boundary problem is recovered with a finite value of W in a mesoscopic scale. They showed that when W is chosen to be small enough, the outcome is almost independent of the value of W. Hence, this model enables us to obtain quantitatively accurate results for a given set of physical parameters. Thus, in this regard, this model is called the quantitative phase-field model.

The development of the quantitative phase-field model for the alloy solidification process was hampered by a difficult problem. Almgren carried out a thin-interface limit analysis for pure materials with unequal diffusivities in the solid and liquid phases and demonstrated that in the case of asymmetric diffusivities, there exist several anomalous effects which scale with W.[115] There are also analogous interface effects involved in the alloy solidification models. In the alloy solidification process, these interface effects modifies the mass conservation law at the interface as follows,[116]

$$c_l^*(1-k)V = D_s \frac{\partial c_s}{\partial n}\bigg|^* - D_l \frac{\partial c_l}{\partial n}\bigg|^* + C_1 + C_2 + C_3, \quad \text{...(13)}$$

where

$$C_1 \propto c_l(1-k)V\kappa W, \quad \text{.....(14)}$$

$$C_2 \propto D_l \frac{\partial^2 c_l}{\partial n^2} W, \quad \text{.....(15)}$$

$$C_3 \propto k c_l (1-k) V^2 W, \quad \text{.....(16)}$$

The magnitudes of the interface effects are proportional to W. The elimination of these effects requires several constraints in interpolating functions such as $f(p)$ and $g(p)$ to be satisfied simultaneously. This results in the stringent restriction in the modeling. However, Karma devised a novel scheme to resolve this problem for a dilute alloy solidification with a zero diffusivity in the solid (a one-sided model).[117] He introduced a phenomenological current term called the antitrapping current term into the diffusion equation. Therefore, the diffusion equation can be written as,

$$\frac{\partial c}{\partial t} = -\nabla(\mathbf{J}_c + \mathbf{J}_{\text{at}}), \quad \text{.....(17)}$$

where $\mathbf{J}_{\text{at}}$ is the antitrapping current given by

$$\mathbf{J}_{\text{at}} = -2a(p)\frac{\varepsilon}{\sqrt{\omega}}(c_l - c_s)\frac{\partial p}{\partial t}\frac{\nabla p}{|\nabla p|}, \quad \text{.....(18)}$$

where $a(p)$ is the interpolating function. This term provides the additional degree of freedom in choosing the form of interpolating functions. Futhermore, it allows one to eliminate all the spurious effects for the one-sided model. This model corresponds to the quantitative phase-field model for the alloy solidification process. This model was extended by Floch and Plapp to include the description of the two

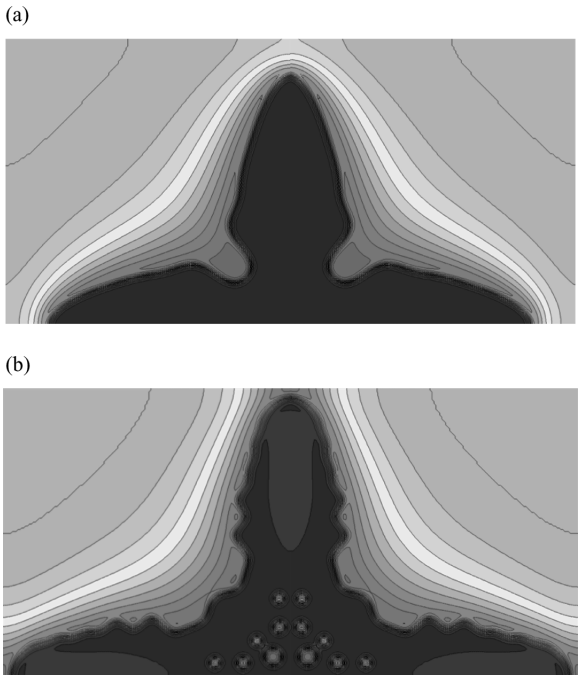

Fig. 7. Dendrites structures during an alloy solidification process calculated by the quantitative phase field model (a) and the same model but without the antitrapping current (b). The value of concentration is distinguished by the different color. The dendrite morphology is quite different and, in particular, the simulation in (b) is unstable, even though the calculation condition is the same in both the cases except for the introduction of the antitrapping current.[121]

phase solidification process.[118,119] Furthermore, it was extend to include the multi-component system by Kim.[120] In addition, the antitrapping current approach was developed for the alloy system with an arbitrary value of the solid diffusivity.[121] The effect of the antitrapping current term on the dendrite structure for an alloy solidification process is demonstrated in **Fig. 7**. Although the calculation conditions are the same in both the models, the substantial difference in the concentration fields and morphology of the interface appears between these results. Overall, the quantitative phase-field models have been increasingly utilized for quantitative simulation of a variety of the solidification processes.[122–131]

5.2. Summary

As mentioned above, the recent development of the quantitative phase-field model enables us to perform the quantitatively accurate simulation for the solidification microstructure. Combined with the recent development of the *in-situ* observation technique, this model is expected to contribute to the progress of our understanding of the solidification phenomena. However, it should be pointed out that the quantitatively accurate simulation requires the input of physical parameters measured with a high precision. The interfacial energy is one of the most important parameters for the phase-field simulation. However, the experimentally measured value of this quantity is prone to generally involve a large uncertainty. In this regard, we would like to refer to the recent attempt for the determination of the solid–liquid interfacial energy based on the Molecular Dynamics (MD) simulation.[132] In addition, the MD estimation of the liquid diffusivity and kinetic coefficient should be quite important task for the quantitative description and prediction of the solidification microstructure.[3,133,134] As mentioned above, the phase-field model for the solidification is quite phenomenological approach. An attempt to put more physics on the phase-field model for the solidification would be a quite challenging and important task. In this regard, we would like to point out the importance of the multi-scale modeling based on the combination of the phase-field model and an atomistic model.

6. Concluding Remarks

The interest of both industry and academia in the methodology for "computer simulations of solidification and casting" has remarkably increased. Today, accurate predictions of the solidification microstructure, directly related to product qualities and material properties, relies heavily upon the establishment of methodologies for macroscopic-scale, mesoscopic-scale and microscopic-scale modeling. Furthermore on the multi-scale modeling based on a combination of these models. In addition, to achieve the goal of the process and material development of advanced alloys for industrial applications, the most significant challenge in the future might be their application to multi-component alloys, through coupling thermodynamic and kinetic databases.

Acknowledgement

Some parts of this work were carried out with a financial grant from the Hugo Carlsson Foundation for Scientific Research, administered by Jernkontoret, Sweden.

REFERENCES

1) D. M. Stefanescu: *ISIJ Int.*, **35** (1995), 637.
2) K. Nakajima: *ISIJ Int.*, **46** (2006), 795.
3) M. Asta, C. Beckermann, A. Karma, W. Kurz, R. Napolitano, M. Plapp, G. Purdy, M. Rappaz and R. Trivedi: *Acta Mater.*, **57** (2009), 941.
4) M. C. Flemings: Solidification Processing, McGraw-Hill, New York, (1976), 244.
5) M. C. Flemings and G. E. Nereo: *Trans. Met. Soc. AIME*, **239** (1967) 1449.
6) M. C. Flemings, R. Mehrabian and G. E. Nereo: *Trans. Met. Soc. AIME*, **242** (1968), 41.
7) N. Streat and F. Weinberg: *Metall. Trans.*, **5** (1974), 2539.
8) R. Mehrabian, M. Keane and M. C. Flemings: *Metall. Trans.*, **1** (1970), 1209.
9) S. Asai, T. Sahara and I. Muchi: *Tetsu-to-Hagané*, **63** (1977), 1512.
10) T. Fuji, D. R. Poirier and M. C. Flemings: *Metall. Trans. B*, **10B** (1979), 331.
11) I. Ohnaka, T. Fukusako and K. Nishikawa: *Tetsu-to-Hagané*, **67** (1981), 547.
12) W. D. Bennor and F. P. Ineropera: *Int. J. Heat Mass Trans.*, **30** (1987), 2161.
13) C. Beckermann: *Int. Mater. Rev.*, **47** (2002), 243
14) L Nastac: Modeling and Simulation of Microstructure Evolution in Solidification Alloys, Springer Verlag, New York, (2004), 14.
15) M. C. Schneider, J. P. Gu, C. Beckermann, W. J. Boettinger and U. R. Kattner: *Mater. Trans. A*, **28A** (1997), 1517.
16) S. D. Felicelli, D. R. Poirier and J. C. Heinrich: *J. Cryst. Growth*, **191** (1998), 879.
17) T. Sawada, K. Oikawa and K. Anzai: Abstract of the 2nd Int. Symposium on Cutting Edge of Computer Simulation of Solidification and Casting, Sapporo, (2010), 21.
18) S. M. Copley, A. F. Giamei, S. M. Johnson and M. F. Hombecker: *Metall. Trans.*, **1** (1970), 2193.
19) K. Suzuki and T. Miyamoto: *Tetsu-to-Hagané*, **63** (1977), 53.
20) T. M. Pollock and W. H. Murphy: *Metall. Mater. Trans. A*, **27A** (1996), 1081.
21) J. R. Sarazin and A. Hellawell: *Metall. Trans. A*, **19A** (1988), 1861.
22) M. I. Bergman, D. R. Feam, J. Bloxham and M. C. Shannon: *Metall. Mater. Trans. A*, **28A** (1997), 859.
23) P. Auburtin, T. Wang, S. L. Cockroft and A. Mitchell: *Metall. Mater. Trans. B*, **31B** (2000), 801.
24) S. Tait and C. Jaupart: *J. Geophys. Res.*, **97** (1992), 6735.
25) M. G. Worster: *J. Fluid Mech.*, **237** (1992), 649.
26) C. Beckermann, J. P. Gu and W. J. Boettinger: *Metall. Mater. Trans. A*, **31A** (2000), 2545.
27) K. Kajikawa, T. Sato and H. Yamada: *Testu-to-Hagané*, **95** (2009), 613.
28) T. Sawada, K. Oikawa, K. Anzai, F. Takahashi, K. Kajikawa and H. Yamada: *J. JFS*, **82** (2010), 142.
29) M. Rappaz and Ch.-A. Gandin: *Acta Metall.*, **41** (1993), 345.
30) Ch.-A. Gandin and M. Rappaz: *Acta Metall. Mater.*, **42** (1994), 2233.
31) Ch.-A. Gandin and M. Rappaz: *Acta Mater.*, **45** (1997), 2187.
32) Ch.-A. Gandin, J.-L. Desbiolles, M. Rappaz and Ph. Thevoz: *Metall. Mater. Trans. A*, **30A** (1999), 3153.
33) Ch.-A. Gandin, G. Guillemot, B. Appolaire and N. T. Niane: *Mater. Sci. Eng. A*, **342** (2003), 44.
34) G. Guillemot, Ch.-A. Gandin, H. Combeau and R. Heringer: *ISIJ Int.*, **46** (2006), 880.
35) G. Guillemot, Ch.-A. Gandin and M. Bellet: *J. Cryst. Growth*, **303** (2007), 58.
36) Ch.-A. Gandin and I. Steinbach: *ASM Handbook: Casting*, **15** (2008), 435.
37) U. Dilthey and V. Pavlik: Proc. of Modeling of Casting, Welding and Advanced Solidification Processes VIII, ed. by B. G. Thomas and C. Beckermann, TMS, Warrendale, PA, (1998), 589.
38) L. Nastac: *Acta Mater.*, **47** (1999), 4253.
39) L. Beltran-Sanchez and D. M. Stefanescu: *Metall. Mater. Trans. A*,

34A (2003), 367.
40) L. Beltran-Sanchez and D. M. Stefanescu: *Metall. Mater. Trans. A*, **35A** (2004), 2471.
41) M. F. Zhu and C. P. Hong: *ISIJ Int.*, **41** (2001), 436.
42) M. F. Zhu and C. P. Hong: *ISIJ Int.*, **42** (2002), 520.
43) M. F. Zhu, S. Y. Lee and C. P. Hong: *Phy. Rev.*, **E69** (2004), 061610.
44) M. F. Zhu and C. P. Hong: *Metall Mater Trans A*, **35A** (2004), 1555.
45) M. F. Zhu and D. M. Stefanescu: *Acta Mater.*, **55** (2007), 1741.
46) D. K. Sun, M. F. Zhu, S. Y. Pan and D. Raabe: *Acta Mater.*, **57** (2009), 1755.
47) S. Y. Pan and M. F. Zhu: *Acta Mater.*, **58** (2010), 340.
48) M. F. Zhu, W. Cao, S. L. Chen, C. P. Hong and Y. A. Chang: *J. Phase Equilibria Diffus.*, **28** (2007), 130.
49) S.-H. Cho, T. Okane and T. Umeda: *Found. Eng.*, **71** (1999), 252.
50) W. Oldfield: *ASM Trans.*, **59** (1966), 945.
51) Y. Natsume and K. Ohsasa: *ISIJ Int.*, **46** (2006), 896.
52) M. Yamazaki, Y. Natsume, H. Harada and K. Ohsasa: *ISIJ Int.*, **46** (2006), 903.
53) Ph. Thevoz, J. L. Desbiolles and M. Rappaz: *Metall. Trans. A*, **20A** (1989), 311.
54) K. Nakajima and S. Mizoguchi: *Bull. Inst. Adv. Mater. Process. Tohoku Univ. (Sozaiken Iho)*, **56** (2000), 107.
55) H. W. Zhang, K. Nakajima, R. Q. Wu, Q. Wang and J. C. He: *ISIJ Int.*, **49** (2009), 1000.
56) H. W. Zhang, K. Nakajima, H. Lei and J. C. He: *ISIJ Int.*, **50** (2010), 1835.
57) D. M. Stefanescu: Science and Engineering of Casting Solidification, Plenum Pub., New York, (2002), 180.
58) W. Kurz and D. J. Fisher: Fundamentals of Solidification (fourth revised edition), Trans. Tech. Pub., Uetikon-Zuerich, (1998), 69.
59) W. Kurz, B. Giovanola and R. Trivedi: *Acta Metall.*, **34** (1986), 823.
60) J. Lipton, W. Kurz and R. Trivedi: *Acta Metall.*, **35** (1987), 957.
61) H. W. Zhang, K. Nakajima, W. Xing, A. L. Wang and J. C. He: *ISIJ Int.*, **49** (2009), 1010.
62) G. H. Gulliver: *J. Inst. Met.*, **9** (1913), 120.
63) G. H. Gulliver: *J. Inst. Met.*, **11** (1914), 252.
64) G. H. Gulliver: *J. Inst. Met.*, **13** (1915), 263.
65) E. Scheil: *Z. Metallkd.*, **34** (1942), 70.
66) E. Kozeschnik: *Metall. Mater. Trans.*, **31A** (2000), 1682.
67) Q. Chen and B. Sundman: *Mater. Trans.*, **43** (2002), 551.
68) A. Borgenstam, A Engström, L. Höglund and J. Ågren: *J. Phase Equilibria*, **21** (2000), 269.
69) T. Helander: MOB Solution Database, V2.0. Thermo-Calc software AB, Stockholm, SE, (2008).
70) S. Kobayashi: *J. Cryst. Growth*, **88** (1988), 87.
71) S. Kobayashi, H. Tomono and K. Gunji: *Trans. Iron Steel Inst. Jpn.*, **28** (1988), 214.
72) S. Kobayashi: *Trans. Iron Steel Inst. Jpn.*, **28** (1988), 535.
73) S. Kobayashi: *Trans. Iron Steel Inst. Jpn.*, **28** (1988), 728.
74) C. Y. Wang and C. Beckermann: *Metall. Trans. A*, **24A** (1993), 2787.
75) C. Y. Wang and C. Beckermann: *Mater. Sci. Eng.*, **171A** (1993), 199.
76) M. A. Martorano, C. Beckermann and Ch.-A. Gandin: *Metall. Mater. Trans. A*, **34A** (2003), 1657.
77) Ch.-A. Gandin, S. Mosbah, Th. Volkmann and D. M. Herlach: *Acta Mater.*, **56** (2008), 3023.
78) D. Tourret and Ch.-A. Gandin: *Acta Mater.*, **57** (2009), 2066.
79) H. W. Zhang, Ch.-A. Gandin, H. B. Hamouda, D. Tourret, K. Nakajima and J. C. He: *ISIJ Int.*, **50** (2010), 1859.
80) M.J.M. Krane, F. Incropera and D. R. Gaskell: *Int. J. Heat Mass Trans.*, **40** (1997), 3827.
81) B. Pustal, B. Böttger, A. Ludwig, P. R. Sahm and A. Bührig-Polaczek: *Metall. Mater. Trans. B*, **34B** (2003), 411.
82) L. Thuinet and H. Combeau: *Comp. Mater. Sci.*, **45** (2009), 294.
83) L. Thuinet and H. Combeau: *Comp. Mater. Sci.*, **45** (2009), 285.
84) Y. Natsume, M. Shimamoto and H. Ishida: *ISIJ Int.*, **50** (2010), 1867.
85) A. Karma: Encyclopedia of Materials Science and Technology, Oxford Elsevier, (2001).
86) L.-Q. Chen: *Annu. Rev. Mater. Sci.*, **32** (2002), 113.
87) W. J. Böttinger, J. A. Warren, C. Beckermann and A. Karma: *Annu. Rev. Mater. Sci.*, **32** (2002), 163.
88) M. Ode, S. G. Kim and T. Suzuki: *ISIJ Int.*, **41** (2001), 1076.
89) I. Steinbach: *Modelling Simul. Mater. Sci. Eng.*, **17** (2009), 07301.
90) R. Kobayashi: *Physica D*, **63** (1993), 410.
91) R. Kobayashi: *Exp. Math.*, **3** (1994), 59.
92) A. A. Wheeler, W. J. Boettinger and G. B. McFadden: *Phys. Rev. A*, **45** (1992), 7424.
93) J. A. Warren and W. J. Boettinger: *Acta Metall.*, **43** (1995), 689.
94) S. G. Kim, W. T. Kim and T. Suzuki: *Phys. Rev. E*, **60** (1999), 7186.
95) I. Steinbach, F. Pezzola, B. Nestler, M. Seeßelberg, R. Prieler, G. J. Schmitz and J. L. L. Rezende: *Physica D*, **94** (1996), 135.
96) G. B. McFadden, A. A. Wheeler, R. J. Braun, S. R. Coriell and R. F. Sekerka: *Phys. Rev. E*, **48** (1993), 2016.
97) A. A. Wheeler, B. T. Murray and R. J. Schaefer: *Physica D*, **66** (1993), 243.
98) S.-L. Wang, R. F. Sekerka, A. A. Wheeler, B. T. Murray, S. R. Coriell, R. J. Braun and G. B. McFadden: *Physica D*, **69** (1993), 189.
99) A. Karma: *Phys. Rev. E*, **49** (1994), 2245.
100) J. Tiaden, B. Nestler, H. J. Diepers and I. Steinbach: *Physica D*, **115** (1998), 73.
101) I. Steinbach and F. Pezzolla: *Physica D*, **134** (1999), 385.
102) B. Neslter, A. A. Wheeler and H. Gracke: *Comput. Mater. Sci.*, **26** (2003), 111.
103) S. G. Kim, W. T. Kim, T. Suzuki and M. Ode: *J. Cryst. Growth*, **261** (2004), 135.
104) B. Böttger, J. Eiken and I. Steinbach: *Acta Mater.*, **54** (2006), 2697.
105) R.S. Qin, E.R. Wallach, R.C. Thomson: *J. Cryst. Growth*, **279** (2005), 163.
106) J. Eiken, B. Böttger and I. Steinbach: *Phys. Rev. E*, **73** (2006), 066122.
107) S. Nomoto, S. Minamoto and K. Nakajima: *ISIJ Int.*, **49** (2009), 1019.
108) G. Caginalp: *Phys. Rev. A*, **39** (1989), 5887.
109) G. Caginalp: *Ann. Phys.*, **172** (1986), 136.
110) G. Caginalp and P. Fife: *Phys. Rev. B*, **34** (1986), 4940.
111) R. Folch, J. Casademunt, A. Hernández-Machado and L. Ramírez-Piscina: *Phys. Rev. E*, **60** (1999), 1724.
112) K. R. Elder, M. Grant, N. Provatas and J. M. Kosterlitz: *Phys. Rev. E*, **64** (2001), 021604.
113) A. Karma and W.-J. Rappel: *Phys. Rev. E*, **53** (1996), R3017.
114) A. Karma and W.-J. Rappel: *Phys. Rev. E*, **57** (1998), 4323.
115) R. F. Almgren: *SIAM J. Appl. Math.*, **59** (1999), 2086.
116) B. Echebarria, R. Folch, A. Karma and M. Plapp: *Phys. Rev. E*, **70** (2004), 061604.
117) A. Karma: *Phys. Rev. Lett.*, **87** (2001), 115701.
118) R. Folch and M. Plapp: *Phys. Rev. E*, **68** (2003), 010602(R).
119) R. Folch and M. Plapp: *Phys. Rev. E*, **72** (2005), 011602.
120) S. G. Kim: *Acta Mater.*, **55** (2007), 4391.
121) M. Ohno and K. Matsuura: *Phys. Rev. E*, **79** (2009), 031603.
122) J.C. Ramirez, C. Beckermann, A. Karma and H.-J. Diepers: *Phys. Rev. E*, **69** (2004), 051607.
123) M. Greenwood, M. Haataja and N. Provatas: *Phys. Rev. Lett.*, **93** (2004), 246101.
124) C. W. Lan and C. J. Shih: *Phys. Rev. E*, **69** (2004), 031601.
125) J. C. Ramirez and C. Beckermann: *Acta Mater.*, **53** (2005), 1721.
126) A. Badillo and C. Beckermann: *Acta Mater.*, **54** (2006), 2015.
127) C. Tong, M. Greenwood and N. Provatas: *Phys. Rev. B*, **77** (2008), 064112.
128) H. Emmerich and R. Siquieri: *J. Phys. Condens. Matter*, **18** (2006), 11121.
129) M. Plapp: *J. Cryst. Growth*, **303** (2007), 49.
130) R. Siquieri and H. Emmerich: *Philos. Mag. Lett.*, **87** (2007), 829.
131) G. Boussinot, E. A. Brener and D. E. Temkin: *Acta Mater.*, **58** (2010), 1750.
132) J. J. Hoyt, M. Asta and A. Karma: *Phys. Rev. Lett.*, **86** (2001), 5530.
133) J. J. Hoyt and M. Asta: *Phys. Rev. B*, **65** (2002), 214106.
134) J. J. Hoyt, M. Asta and A. Karma: *Mater. Sci. Eng.*, **R41** (2003), 121.